

Temperature profile for Poiseuille flow

B. D. Todd and Denis J. Evans

Research School of Chemistry, Australian National University, GPO Box 414, Canberra, Australian Capital Territory 2601, Australia

(Received 10 June 1996)

For planar Poiseuille flow of an atomic fluid in the weak-flow regime, we find that the classical Navier-Stokes prediction of a quartic temperature profile is incorrect. Our results, which confirm a prediction made by Baranyai, Evans, and Daivis (BED) [Phys. Rev. A **46**, 7593 (1992)], indicate that near the center of the channel the temperature profile is quadratic. When the temperature profile is fitted to the theoretical predictions of BED we obtain estimates of the thermal conductivity that are in excellent agreement with accurate independent estimates of this transport coefficient. If the presence of the quadratic component of the temperature profile is ignored, the derived value of the thermal conductivity is in error by some 50%. [S1063-651X(97)07903-8]

PACS number(s): 03.40.Gc, 02.50.-r, 51.10.+y, 05.70.Ln

I. INTRODUCTION

In a previous paper Baranyai, Evans, and Daivis (BED) [1] used molecular-dynamics computer simulation to show that in the presence of a spatially varying strain rate, heat flow can occur even in the *absence* of a temperature gradient ∇T . It was observed that such a heat flux J_Q is proportional to the gradient of the square of the strain rate $J_Q \propto \nabla \dot{\gamma}^2$. This simple observation has profound consequences for our understanding of heat transport in systems subject to viscous heating.

Consider heat transport in a system undergoing Poiseuille flow between two parallel walls that are maintained at a common fixed temperature. An external force F_e (such as gravity) drives the flow, which in turn generates viscous heat. This viscous heat is proportional to the square of the local strain rate $\dot{\gamma}(y)^2$ (y is the normal coordinate) and in turn generates local variations in the temperature. Fourier's law then predicts that these temperature inhomogeneities will induce a local heat flux $J_Q \propto \nabla T(y)$. However, BED predicted that even in the absence of local variations in the temperature $\nabla T=0$ spatial variations in the strain rate will also generate a heat flux $J_Q \propto \nabla \dot{\gamma}^2$. In the weak flow limit ($F_e \rightarrow 0$), these two contributions to the heat flux (Fourier's contribution and the shear gradient contribution, respectively) clearly have the same dependence on the applied field. Neither contribution dominates the other in this limit.

In Ref. [1] BED predicted that when both of these contributions are accounted for, the normal variation of the temperature across a Poiseuille channel deviates from the weak flow prediction of the classical Navier-Stokes momentum and heat equations, namely, $T \sim y^4$. Instead, when the shear gradient contributions to the heat flux are included the temperature profile contains contributions that are quadratic in the normal coordinate. These quadratic contributions are only observable over microscopic distances near the center of the channel. This is presumably why the effect has not, to our knowledge, been seen experimentally. In Ref. [1] BED did not simulate Poiseuille flow, but instead carried out simulations of shear flow driven by a transverse external field (a so-called sinusoidal transverse field). This technique permits the simulation of inhomogeneous shear flow without the added complications of modeling walls.

The price paid for this simplification was that a fictitious (i.e., not occurring in nature) thermostat had to be introduced into the simulation to remove the viscous heat. This thermostat enabled the observation of heat flow in an inhomogeneously shearing system where the temperature was constant everywhere. One might argue that the "excess" heat observed could have been induced by the thermostating mechanism itself and that for a natural system, where no such fictitious thermostats exist, the usual Fourier heat conduction law would remain valid.

In the present paper we address this criticism by carrying out molecular-dynamics computer simulations of planar Poiseuille flow between parallel isothermal atomic walls. The equations of motion for the fluid atoms between the walls are simply Newton's equations for interacting particles subject to an external gravity field that drives the flow. The system we study is an atomic fluid sandwiched between thermostatted atomic walls. We have recently developed efficient exact methods for computing the local thermodynamic flux tensors in such systems [2–5]. We will show that the temperature profile for this system deviates significantly from that predicted by classical Navier-Stokes theory. We also show that an estimate of the thermal conductivity obtained from the quartic fit of the classical Navier-Stokes temperature profile yields an erroneous value of the estimated thermal conductivity.

The comparisons that we make of the Navier-Stokes predictions of the temperature profile in Poiseuille flow take due account of the effects of the local variations in the transport coefficients that result from viscous heating. In the weak-flow limit these variations can be ignored. Our simulations are carried out close to the weak-field limit so that these variations can be treated as small ($\sim 1\%$) perturbations to the weak-flow Navier-Stokes solution. For the external fields studied in our simulations the spatial variations in the viscosity (η) and thermal conductivity (λ) cannot explain the temperature profile observed in our simulations. In particular, allowance for spatial variations in the viscosity and thermal conductivity cannot explain the quadratic variation of temperature that we observe. Finally, we discuss the implications of shear-induced heat flow within the context of a different definition of a nonequilibrium thermodynamic temperature and find that the heat flux may be writ-

ten in terms of the gradient of this nonequilibrium temperature.

II. THEORY

A. Classical formulation

Consider steady shear flow in the x direction with a velocity gradient $\partial u_x/\partial y \equiv \gamma$ in the y direction. The hydrostatic pressure p , which is a function of temperature T and number density, n , must satisfy the equation

$$\frac{d}{dy} p(y) = 0. \quad (1)$$

In writing this equation we assume that we are sufficiently close to equilibrium for local thermodynamic equilibrium to hold. If the flow is driven by an external force F_e (such as gravity) that acts on individual atoms in the fluid, the steady-state momentum conservation equation implies [2]

$$\frac{d}{dy} P_{xy}(y) \equiv -\frac{d}{dy} \left[\eta(y) \frac{du_x(y)}{dy} \right] = n(y) F_e, \quad (2)$$

where P_{xy} is the xy element of the pressure tensor, η is the shear viscosity, and n is the number density. The steady-state Navier-Stokes energy equation is

$$\begin{aligned} \frac{dJ_{Qy}(y)}{dy} + P_{xy}(y) \gamma(y) &= -\frac{d}{dy} \left[\lambda(y) \frac{dT(y)}{dy} \right] - \eta(y) \gamma(y)^2 \\ &= 0, \end{aligned} \quad (3)$$

where T is the temperature, J_{Qy} is the y component of the heat flux vector, and λ is the thermal conductivity.

In the weak-flow limit, the local variation of thermodynamic properties and transport coefficients (caused by viscous heating) may be ignored and Eq. (3) reduces to $\lambda d^2 T(y)/dy^2 + \eta \gamma(y)^2 = 0$. In the case of planar Poiseuille flow where the fluid flows in the x direction between two stationary parallel plates separated in the y direction by a distance l_y , we can solve Eqs. (2) and (3) in the weak-flow limit, giving a velocity profile

$$u_x(y) = -\frac{nF_e}{2\eta} \left(y^2 - \frac{l_y^2}{4} \right) \equiv u_0 + u_2 y^2 \quad (4)$$

and a temperature profile

$$T(y) = T_0 + T_4 y^4, \quad (5)$$

where $T_4 = -(nF_e)^2/12\lambda\eta$ and T_0 is the temperature at the channel midplane $y=0$.

In writing this equation we assume that the transport coefficients are constant over the channel width and that the heat flux is linearly proportional to the temperature gradient (i.e., Fourier's law $\mathbf{J}_q = -\lambda \nabla T$). Clearly, the first of these assumptions will break down in very narrow channels where the effects of molecular packing manifest themselves in an oscillatory variation of almost all properties, including the number density [2–5]. In the present work we are interested in only relatively wide channels where molecular packing

effects are unimportant and where continuum mechanics is expected to give an accurate description of the system.

The first corrections to the continuum weak-field solutions for Poiseuille flow might be expected to arise from the variations induced in the transport coefficients by the temperature and density variations that are brought on by viscous heating in the flow itself. For our geometry, all thermodynamic quantities are functions of y alone. The pressure is a function of both ρ and T , but Eq. (1) implies

$$\frac{dp}{dy} = \frac{\partial p}{\partial \rho} \frac{d\rho}{dy} + \frac{\partial p}{\partial T} \frac{dT}{dy} = 0. \quad (6)$$

Since $\partial p/\partial \rho$ and $\partial p/\partial T$ are constant coefficients, the variations in density and temperature are proportional $\Delta \rho \propto \Delta T$. In the linear regime the leading order variation in the temperature is quartic, so the density variations must also be quartic, $\Delta \rho \propto \Delta T \propto y^4$. Knowing the functional variation of density and temperature allows us to determine the form of the variation of $\eta(y)$ and $\lambda(y)$ in an analogous manner. Thus we can write, to a first approximation,

$$\begin{aligned} n(y) &= n_0 + n_4 y^4, \\ \eta(y) &= \eta_0 + \eta_4 y^4, \\ \lambda(y) &= \lambda_0 + \lambda_4 y^4, \end{aligned} \quad (7)$$

where $n_0, n_4, \eta_0, \eta_4, \lambda_0, \lambda_4$ are constants.

If we substitute these spatially varying transport coefficients into Eqs. (2) and (3) and solve for $u_x(y), T(y)$ we will arrive at a temperature profile that now takes into account the variations in space of η and λ . Ideally we should iterate this process until convergence; however, we shall see later that for the flow rates studied in this work we can stop the process after the first iteration. Solving Eq. (3) with the values of $\eta(y)$ and $\lambda(y)$ in Eq. (7) gives us

$$T(y) = T_0 + T_4 y^4 + T_8 y^8 + O(y^{12}), \quad (8)$$

$$T_4 = -\frac{u_2^2 \eta_0}{3\lambda_0}, \quad T_8 = -\frac{u_2^2 (3\lambda_0 \eta_4 - 7\lambda_4 \eta_0)}{42\lambda_0^2}, \quad (9)$$

where again T_0 is the midchannel temperature (at $y=0$).

Equation (8) currently has five unknowns ($\eta_0, \eta_4, \lambda_0, \lambda_4, T_0$), but this can be reduced to three by noting that the viscosity $\eta(y)$ can be calculated explicitly. In Ref. [2] we showed that for planar Poiseuille flow the shear stress P_{xy} could be calculated in a molecular-dynamics simulation directly by integrating Eq. (2),

$$P_{xy}(y) = F_e \int_0^y dy' n(y'), \quad (10)$$

where $n(y)$ is the spatially dependent number density. Using Eq. (7) we can write P_{xy} as

$$P_{xy}(y) = F_e (n_0 y + \frac{1}{5} n_4 y^5), \quad (11)$$

where the constant of integration is zero [2]. In the local equilibrium regime we find

$$\eta(y) = -\frac{F_e}{2u_2} \left(n_0 + \frac{1}{5} n_4 y^4 \right). \quad (12)$$

In deriving Eq. (12) we are assuming that the length scale characteristic of variations in the strain rate is much greater than the range of the intermolecular potential. This assumption justifies the use of a local constitutive relation for the shear viscosity $\eta(y)$. Thus $\eta_0 = -F_e n_0 / 2u_2$ and $\eta_4 = -F_e n_4 / 10u_2$. The coefficients n_0 and n_4 can be obtained directly from computer simulation, as can the temperature coefficients, and so Eq. (8) has only three unknowns. Thus we can fit Eq. (8) to the temperature profile to determine the best estimates of λ_0 , λ_4 , and T_0 .

B. Strain rate coupling

The heat flux constitutive relation postulated by BED [1] was

$$\mathbf{J}_Q = -\lambda \nabla T - \xi \nabla [\nabla \mathbf{u} : (\nabla \mathbf{u})^T], \quad (13)$$

where ξ is a phenomenological strain rate coupling coefficient, λ is the thermal conductivity coefficient, and \mathbf{u} is the streaming velocity of the fluid. It is possible that other terms with the same symmetry as our strain rate coupling term could also make contributions to the heat flux. However, from the work of BED [1] we know that these additional couplings do not involve higher-order derivatives of the temperature field. This is because BED demonstrated the existence of a heat flux in the absence of *any* temperature variations. Also one may consider couplings to the stress tensor rather than to the strain rate tensor as in Eq. (13). However, writing Eq. (13) in terms of stress couplings simply amounts to a redefinition of ξ since in the weak-field limit, stress is simply proportional to strain rate. The couplings cannot involve couplings to the hydrostatic pressure since in the weak-field limit mechanical stability demands that the hydrostatic pressure must be constant.

In the case of planar shear flow of a simple fluid, Eq. (13) can be written as

$$J_{Qy}(y) = -\lambda(y) \nabla_y T(y) - \xi(y) \nabla_y \gamma(y)^2. \quad (14)$$

For our Poiseuille flow geometry we have [1,4] instead of Eq. (3)

$$\frac{d}{dy} \left[\lambda(y) \frac{dT(y)}{dy} \right] + \frac{d}{dy} \left[\xi(y) \frac{d\gamma(y)^2}{dy} \right] + \eta(y) \gamma(y)^2 = 0. \quad (15)$$

Equation (15) is a fourth-order differential equation that requires four independent boundary conditions for its solution. This is an example of a notorious problem in hydrodynamics beyond the Navier-Stokes order. We avoid this difficulty by applying a perturbation expansion. The fourth order terms in Eq. (15) act on only lower-order solutions that are known already. At each order, the equation for the unknown function remains of second order.

In the weak-flow limit where the spatial variation of the transport coefficients may be ignored we have instead of Eq. (5)

$$T(y) = T_0 + T_2 y^2 + T_4 y^4, \quad (16)$$

where the coefficients are given as $T_2 = -(nF_e)^2 \xi / \lambda \eta^2$ and $T_4 = -(nF_e)^2 / 12\lambda \eta$ [4]. As was pointed out by BED, the quadratic term dominates over the quartic term whenever $y \ll \sqrt{12\xi/\eta}$. Both terms in Eq. (16) have the same functional dependence on the external field, thus even in the zero-field limit, nonclassical behavior resulting from the effects of strain rate coupling will be observed. In this limit the characteristic length that controls the crossover from classical to nonclassical behavior is independent of the magnitude of the external field driving the flow.

Following similar arguments to those given in Sec. II A above, to a first approximation the number density varies as $n(y) = n_0 + n_2 y^2 + n_4 y^4$. Hence the spatial variation of the transport coefficients may be represented as

$$\begin{aligned} \eta(y) &= \eta_0 + \eta_2 y^2 + \eta_4 y^4, \\ \lambda(y) &= \lambda_0 + \lambda_2 y^2 + \lambda_4 y^4, \\ \xi(y) &= \xi_0 + \xi_2 y^2 + \xi_4 y^4. \end{aligned} \quad (17)$$

Allowing a quadratic variation in the streaming velocity

$$u_x(y) = u_0 + u_2 y^2 + O(y^4) \quad (18)$$

and substituting Eqs. (17) into (15) gives

$$T(y) = T_0 + T_2 y^2 + T_4 y^4 + T_6 y^6 + O(y^8), \quad (19)$$

where the coefficients are given as

$$\begin{aligned} T_2 &= -4 \frac{u_2^2 \xi_0}{\lambda_0}, \\ T_4 &= -\frac{u_2^2 (\lambda_0 \eta_0 + 6\lambda_0 \xi_2 - 6\lambda_2 \xi_0)}{3\lambda_0^2}, \\ T_6 &= -\frac{2u_2^2 (30\lambda_0^2 \xi_4 + 3\lambda_0^2 \eta_2 + 30\lambda_2^2 \xi_0 - 30\lambda_0 \lambda_4 \xi_0 - 5\lambda_2 \lambda_0 \eta_0 - 30\lambda_2 \lambda_0 \xi_2)}{45\lambda_0^3}. \end{aligned} \quad (20)$$

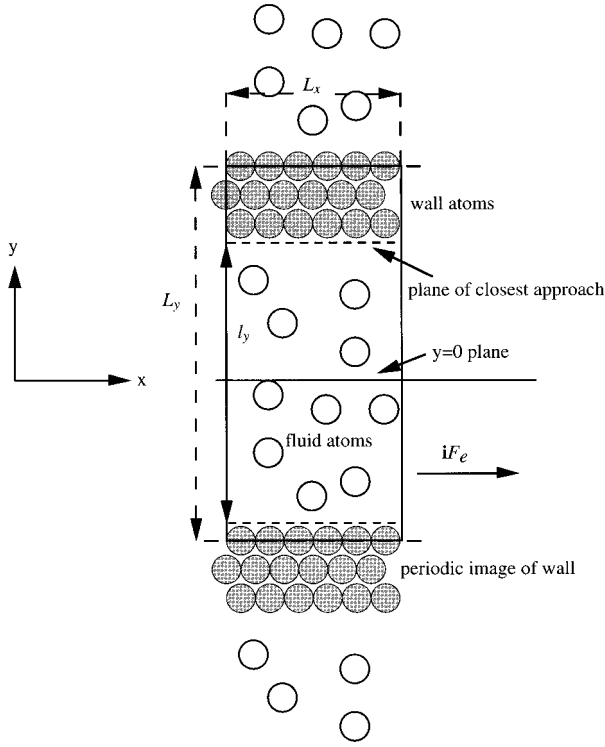


FIG. 1. Simulation geometry for planar Poiseuille flow. The z axis is normal to the page.

In the above derivation we have allowed for only a quadratic variation in the velocity because it is easy to show that the ratio u_4/u_2 is proportional to F_e^2 . For the field strength used in this work this ratio is only 2.5×10^{-5} . This means that the higher-order terms are negligible compared to the statistical noise. From Eqs. (19) and (20) we can identify which components arise from cross coupling of the heat flux with the strain rate gradient and which components arise from the spatial variations induced by viscous heating in η, λ, ξ . We see that the quadratic term derives solely from the strain rate coupling. The quartic term contains the classical weak-field Navier-Stokes contribution, but also contains contributions from the second-order variation of ξ with distance as well as a component from zeroth-order strain rate coupling and second-order variations of the thermal conductivity with distance (λ_2). Similarly, the sixth-order term contains contributions from η, λ , and ξ . For notational convenience we will refer to the classical weak-field Navier-Stokes solutions given in Eqs. (4) and (5) as NS, to the stronger-field solutions where the spatial variation of transport coefficients is allowed for Eqs. (8) and (9) as YNS, to the weak-field solution including strain rate coupling (16) as XNS, and to the stronger-field strain rate coupling expressions (19) and (20) as XYNS.

III. SIMULATION DETAILS

We have previously described in detail the NEMD techniques used to simulate planar Poiseuille flow [2,3] and here we only briefly outline the way in which the simulations were carried out. The geometry of the system is shown in Fig. 1. Both the fluid and wall particles interact via the Weeks-Chandler-Andersen (WCA) interatomic potential

function [6] $\phi(r) = 4(r^{-12} - r^{-6}) + 1$ for $r < 2^{1/6}$ and $\phi(r) = 0$ for $r > 2^{1/6}$ (we have defined the WCA potential constants σ and ϵ to be unity for simplicity; we also define the fluid and wall particle masses to be unity).

The system was surrounded by periodic images of itself in each of the three Cartesian dimensions. We note here that the simulation geometry is such that the external field is in the x direction and heat will flow in the y direction only. Our system consisted of 1278 fluid atoms bounded by 54 wall atoms that were three atomic layers thick (18 atoms per layer). The walls were separated in the y direction by a length $l_y = 69$ and were fixed in a fcc lattice structure by a combination of restoring forces and a constraint mechanism that fixed the center of mass of each layer of wall particles while allowing individual wall atoms the freedom to vibrate about their lattice sites [2,7]. There was only one three-atom-thick wall per simulation cell. The second wall was simply the periodic image of the first. This periodicity also ensured that the total density of the system remained constant. For details of the governing equations of motion and the integrating scheme used to solve them, the reader is referred to Refs. [2, 3].

The average number density of the system was $\bar{n} = 0.839$. The unit cell dimensions L_x, L_y , and L_z , were 4.6840, 71.9444, and 4.6840 respectively. It is important to note that L_y includes the fluid and wall particles (see Fig. 1).

The walls were kept at a constant temperature of 0.722 and density of 0.8442. The wall temperature was held constant by application of a Gaussian thermostat, which ensured that the average temperature of all the wall atoms was constant. We stress again that even though a thermostat is applied to the wall atoms enabling the removal of viscous heat from the system, the fluid atoms themselves are *not* subject to any thermostat. Their equations of motion are simply Newton's equations for a group of interacting particles subject to an external "gravitational" field F_e that drives the flow between the plates. The external field was weak $F_e = 0.005$, ensuring that the system remained close to the weak-flow limit. The system was first allowed to attain steady state before a simulation of 1.18×10^7 time steps ($\Delta t = 0.001$) was carried out to accumulate data.

Both the temperature and velocity profiles of the fluid were calculated in bins of finite volume $V_{\text{bin}} = L_x \Delta_y L_z = 6.1432$, where $\Delta_y = 0.28$, and at planes with separation Δ_y [5]. In what follows we show only the results calculated in bins because of their superior statistics, but both methods produced identical results within statistical errors.

In Refs. [2, 3] it was shown that a second-order symmetric polynomial provided a good representation of the streaming velocity of the fluid in the zero-flow-rate limit and we show this profile in Fig. 2. However, in this work we consider not only this case, but also higher-order symmetric terms up to $O(y^6)$.

The temperature in each bin was calculated as

$$\langle T(y_{\text{bin}}) \rangle = \frac{\left\langle \sum_{i \in \text{bin}} m_i [\mathbf{v}_i - \mathbf{u}(y, t)] [\mathbf{v}_i - \mathbf{u}(y, t)] \right\rangle}{\langle 3N_{\text{bin}} - d(N_{\text{bin}}/N) \rangle}, \quad (21)$$

where \mathbf{v}_i is the laboratory velocity of particle i , $\mathbf{u}(y, t)$ is the

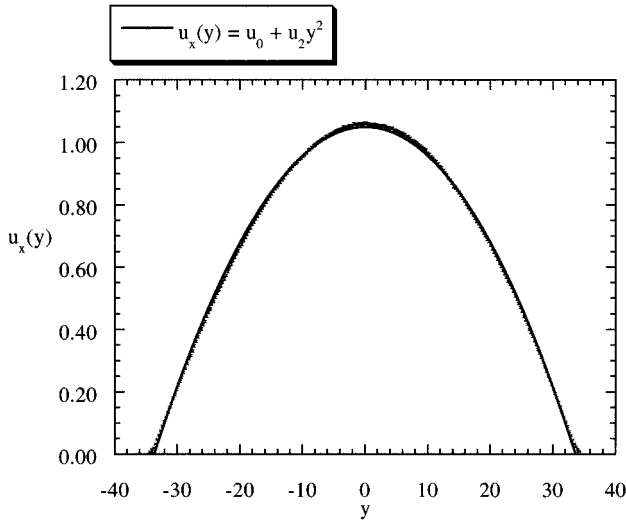


FIG. 2. Streaming velocity profile, showing an $O(y^2)$ symmetric polynomial fit.

instantaneous streaming velocity at y , N_{bin} is the number of particles in any particular bin, N is the total number of fluid particles, d is the number of degrees of freedom lost to the system by fitting the streaming velocity profile, and Boltzmann's constant is equal to 1. The streaming velocity is calculated at each time step by a least-squares fit to the instantaneous velocity profile [2]. Since $d=k/2+1$ degrees of freedom are lost in fitting the coefficients of the streaming velocity to a symmetric polynomial of order k , a factor of dN_{bin}/N degrees of freedom are lost in each bin. This number is very small in comparison to $3N_{\text{bin}}$ and could even be ignored for a simulation of this size. We note here that the angular brackets denote time averages.

As mentioned above, the temperature profile was calculated assuming streaming velocity profiles that were $O(y^2)$, $O(y^4)$, and $O(y^6)$. However, the three corresponding temperature profiles were found to agree within statistical uncertainties, confirming that any deviations to the classically expected temperature profile are *not* a result of inaccurate fitting of the streaming velocity data.

IV. RESULTS AND DISCUSSION

A. Temperature and thermal conductivity

In Fig. 3(a) we show the temperature profile across the entire channel. The data have been symmetrized and smoothed over four bins (i.e., a width of 1.12). Also shown are the fits to this data given by NS and XNS, i.e., assuming constant values of η , λ , and possibly ξ . In Fig. 3(b) we show only the central region of the channel between $-25 \leq y \leq 25$. On this scale it is easy to see that the classical Navier-Stokes solution of a quartic temperature profile does not fit the data well. Including the strain rate coupling term into the temperature equation, as in Eq. (16), generates an additional quadratic term, which fits the data well in the central region.

In Table I we show the values of the coefficients for both the velocity and temperature profiles, as well as the values of the calculated transport coefficients. The viscosity η_0 was calculated directly from the coefficient of the velocity profile, i.e., $\eta_0 = -nF_e/2u_2$, and this value is then used in Eqs.

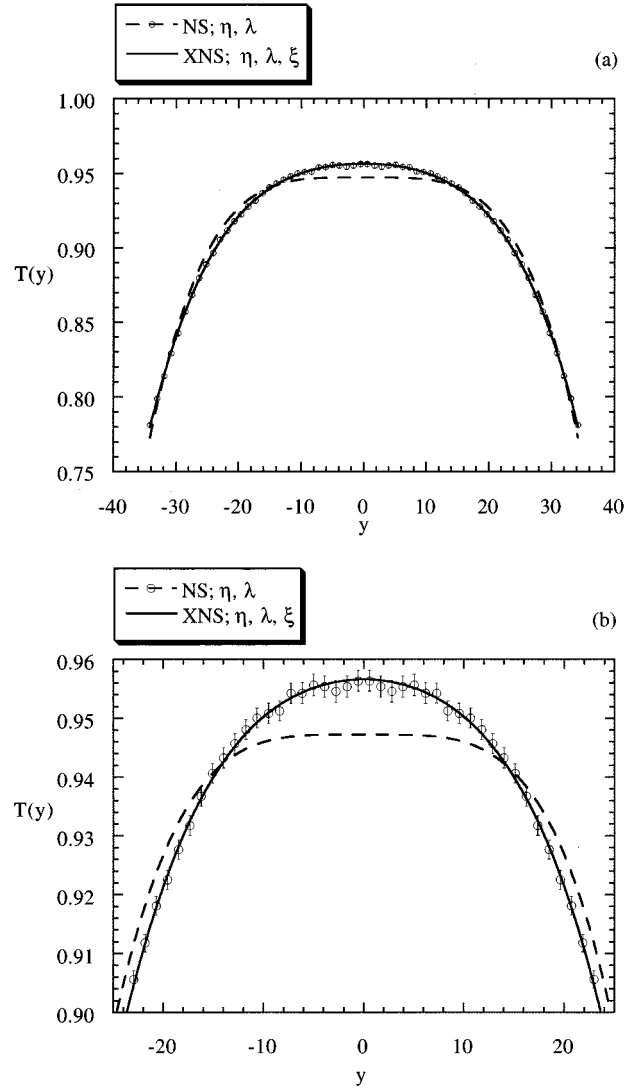


FIG. 3. (a) Temperature data across the entire channel, including the Navier-Stokes (NS) and strain rate coupled Navier-Stokes (XNS) fits to the data. No allowance is made for the effects of viscous heating on the transport coefficients. (b) Temperature data for the region $-25 \leq y \leq 25$, including the NS and XNS fits to the data.

(5) and (16) to find values of λ_0 and ξ_0 . Also shown is the value of the residual R for both temperature fits, which clearly shows that the inclusion of strain rate coupling gives a much better fit to the data.

The value of λ computed from Eqs. (5) and (16) can be compared to the known value of λ calculated by the Evans NEMD thermal conductivity algorithm [8] for a fluid at a state point equal to the temperature and density of the middle of the channel. The state point used was thus $(n, T) = (0.836, 0.955)$ and the simulations were performed for a system of 500 WCA fluid atoms. The thermal conductivity λ_{NEMD} was determined by running a series of simulations at various field strengths and then extrapolating the value of λ_{NEMD} to the zero-field limit. This gave us a value of $\lambda_{\text{NEMD}} = 6.89 \pm 0.05$. From Table I we see that the weak-flow Navier-Stokes estimate is $\lambda_{\text{NS}} = 5.07$, whereas the strain rate coupling Navier-Stokes estimate (i.e., including the strain rate coupling term) gives $\lambda_{\text{XNS}} = 7.90$. The former underestimates the true ther-

TABLE I. Properties of interest for the case of constant transport coefficients (the NS and XNS systems).

System	n	u_2	T_2	T_4	η_0	λ_0	ξ_0	T_0	R
NS	0.839	-9.26×10^{-4}		-1.2803×10^{-7}	2.26	5.07		0.947	0.995 93
XNS	0.839	-9.26×10^{-4}	-5.5185×10^{-5}	-8.2155×10^{-8}	2.26	7.90	126	0.957	0.999 92

mal conductivity by 26.4%, whereas the latter overestimates it by 14.6%. Also we note that the NS solution underestimates T_0 by about 1%, a value outside the range of the error bars of the data, whereas the XNS solution predicts T_0 with very good accuracy.

We now consider the case where the transport coefficients are allowed to vary with position (i.e., y). This gives two data sets: first YNS, which uses y -dependent transport coefficients in the Navier-Stokes equations, and second XYNS, which employs strain rate coupling of the heat flux and y -dependent transport coefficients. The various transport coefficients are given in Table II, along with T_0 and R , while the corresponding fits to the temperature data are plotted in Figs. 4(a) and 4(b). Once again we see from the shape of the profiles that the XYNS fit gives a better fit to the data than the YNS fit. The transport coefficient we are most concerned with is λ_0 , which we find to be $\lambda_{0\text{YNS}}=3.89$ and $\lambda_{0\text{XYNS}}=6.93$. Thus we see that including the spatial variation of the transport coefficients improves the fit of the temperature profile, but does this at the expense of a significantly poorer estimate of the thermal conductivity. The YNS estimated thermal conductivity is only 56% of the known value. This error is much greater than the estimated statistical uncertainties in the data. However, including the spatial variations and strain rate coupling in the heat equation [i.e., Eqs. (19) and (20)] gives us a value that is within 1% of the known thermal conductivity.

The correct thermal conductivity λ_0 , as the correct shape of the temperature profile, and the correct value of the mid-channel temperature T_0 are predicted using the full XYNS solution. Merely accounting for the spatial variation in η and λ alone is *not* sufficient to explain the shape of the temperature profile or the discrepancies in the values of λ_0 or T_0 .

In Sec. II it was noted that the process of determining the functional form of $\eta(y)$, $\lambda(y)$, and $\xi(y)$ should be iterative. Further iterations are unnecessary given the statistical uncertainties in the base data. In Table II we show entries designated as u4XYNS, which were obtained using a second iteration. We do not give the equations corresponding to Eqs. (18)–(20) as the expressions for the coefficients are quite complex. The second iteration allows a fourth-order variation in the streaming velocity, the coefficients for which are given in Table II. From that table we can see that the goodness of fit to the velocity profile does improve somewhat. However, the goodness of fit to the temperature profile does not improve at all. The differences between the ξ_0 values for XYNS and u4XYNS gives an estimate for the statistical uncertainties in ξ_0 . We therefore estimate ξ_0 as 80 ± 20 .

We also note here that the truncation of the series expansion in Eqs. (19) and (20) was tested by considering the residuals of the fit to the temperature data. The eighth-order term in Eq. (19) was explicitly evaluated and the residual for the temperature fit determined. It was found that this residual decreased slightly, suggesting the series converges rapidly

and is adequately truncated at sixth order. We also point out that the sixth-order term must be included in the expansion to enable a complete determination of all the transport coefficients.

B. Heat flux and nonequilibrium temperature

In a previous paper [4] we demonstrated that for a fluid undergoing planar Poiseuille flow, the heat flux remains unchanged from its classical cubic profile by the inclusion of the cross coupling term in the linear constitutive equation for the heat flux. We will now show that this result is in fact general for fluids undergoing planar flow. For simplicity we assume that η and λ are constant.

Consider an arbitrary weak flow planar strain rate profile $\gamma(y)$. Because the flow is weak we may ignore the effects that viscous heating has on the transport coefficients. From the energy equation (15) for such a flow we see that in the steady state

$$\frac{dT(y)}{dy} = -\frac{\eta}{\lambda} \int_0^y \gamma^2(y') dy' - \frac{\xi}{\lambda} \frac{d\gamma^2}{dy}, \quad (22)$$

where we have used the symmetry about the center of the flow ($y=0$) to eliminate the integration constant. This equation may be integrated one more time to give the temperature profile $T(y)$. This profile will clearly be dependent on the value of the strain rate coupling coefficient ξ . We can also calculate the heat flux vector assuming the generalized constitutive relation (13) and (14). This gives,

$$J_Q(y) = -\eta \int_0^y \gamma^2(y') dy'. \quad (23)$$

This is clearly the same expression we would have derived had we not known about the phenomenon of strain rate coupling. Thus we see that strain rate coupling affects the temperature profile, but not the heat flux vector.

As far as measurable thermodynamic quantities are concerned, we could have derived exactly the same temperature and heat flux profiles by defining a new nonequilibrium temperature T_{ne}

$$T_{\text{ne}} = T_{\text{eq}} + \frac{\xi}{\lambda} \gamma^2 \quad (24)$$

and *not* invoking a generalized constitutive relation for heat flow. Indeed, this has recently been noticed by Casas-Vasquez and Jou [9] and Bidar, Casas-Vasquez, and Jou [10].

V. CONCLUSION

We have provided convincing numerical evidence that the classical fourth-order temperature profile generated by vis-

TABLE II. Properties of interest for the case of spatially variant transport coefficients (the YNS and XYNS systems).

System	n_0	n_2	n_4	η_0	η_2	η_4	λ_0	λ_2	λ_4	ξ_0	ξ_2	T_0	R
YNS	0.836		2.179×10^{-8}	2.25		1.173×10^{-8}	3.89		1.476×10^{-8}				0.951
	u_0	u_2	u_4	R									0.999 13
XYNS	1.0494	-0.000 93		0.999 32									
	0.836	7.530×10^{-8}	1.160×10^{-8}	2.25	6.755×10^{-6}	6.244×10^{-9}	6.93	1.795×10^{-4}	2.016×10^{-6}	94.1	0.0389	-3.174×10^{-4}	0.956
u4XYNS	u_0	u_2	u_4	R									0.999 94
	1.0494	-0.000 93		0.999 32									
u4XYNS	0.836	7.530×10^{-8}	1.160×10^{-8}	2.25	6.755×10^{-6}	6.244×10^{-9}	7.102	-4.4×10^{-4}	-2.096×10^{-6}	69.7	0.0080	3.31×10^{-5}	0.956
	u_0	u_2	u_4	R									0.999 94
	1.0682	-0.001 09	1.6141×10^{-7}	0.999 92									

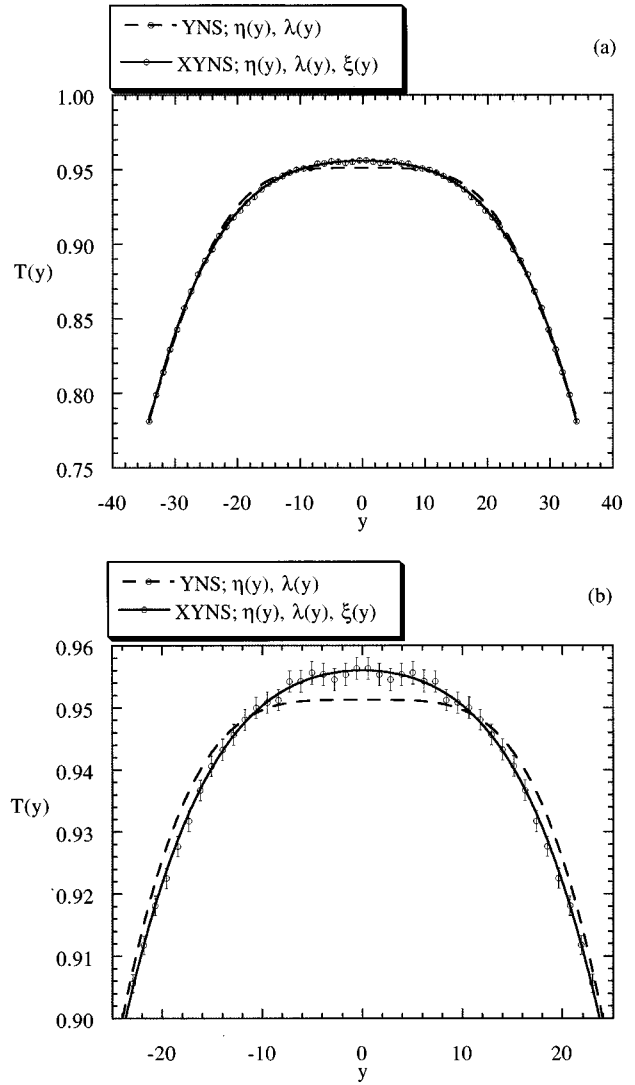


FIG. 4. (a) Temperature data across the entire channel, allowing for y -dependent transport coefficients (YNS) and strain rate coupling (XYNS) fits to the data. y -dependent transport coefficients result from the effects at finite flow rates of viscous heating. (b) Temperature data for the region $-25 \leq y \leq 25$, including the YNS and XYNS fits to the data.

cus heating within Poiseuille flow is incorrect. We have confirmed the prediction of Baranyai, Evans, and Davis [1] that in the weak-flow regime there is a quadratic as well as a quartic component to the temperature profile. One explanation for this is that for weak flows there is a contribution to the heat flux that is proportional to the gradient of the square of the strain rate. Certainly such an effect was seen in computer simulations of sinusoidal shear flow by BED [1] and also in recent more accurate studies by Todd, Evans, and Davis [11]. An alternative, but equivalent, explanation of the origin of the quadratic component to the temperature profile is that the nonequilibrium temperature of a system contains a contribution that is quadratic in the local value of the shear rate (24).

In a previous paper [4] we showed that for planar Poiseuille flow, an analysis of the heat flux vector alone cannot confirm the existence of this strain rate coupling effect. We have now extended this proof to the case of any simple fluid

undergoing *any* planar flow (where the streaming velocity, and hence strain rate, may be expressed as a function of one Cartesian coordinate).

Nothing is known about the variation of the strain rate coupling coefficient ξ with temperature and density. Very little is known about the variation of this coefficient with respect to the thermodynamic force $\partial\gamma^2/\partial y$. We note that the work described in the present paper gives values of the strain rate coupling coefficient ξ that were obtained for values of $\partial\gamma^2/\partial y$ that are two to three orders of magnitude smaller than the smallest values studied by BED [1]. We hope that the present paper stimulates interest towards increasing our

understanding of this coefficient and also its possible relationship to generalized irreversible thermodynamics.

ACKNOWLEDGMENTS

We gratefully acknowledge the assistance of Dr. Debra Searles for programming assistance on the Evans thermal conductivity algorithm, Dr. Harold Schranz for his help in the use of MATHEMATICA, and Dr. Dennis Isbister for his help with MAPLE programming. We also thank the Australian National University Supercomputer Facility for a substantial allocation of computer time.

-
- [1] A. Baranyai, D. J. Evans, and P. J. Daivis, Phys. Rev. A **46**, 7593 (1992).
[2] B. D. Todd, D. J. Evans, and P. J. Daivis, Phys. Rev. E **52**, 1627 (1995).
[3] B. D. Todd, P. J. Daivis, and D. J. Evans, Phys. Rev. E **51**, 4362 (1995).
[4] B. D. Todd and D. J. Evans, J. Chem. Phys. **103**, 9804 (1995).
[5] P. J. Daivis, K. P. Travis, and B. D. Todd, J. Chem. Phys. **104**, 9651 (1996).
[6] J. D. Weeks, D. Chandler, and H. C. Andersen, J. Chem. Phys. **54**, 5237 (1971).
[7] J. G. Powles, S. Murad, and P. V. Ravi, Chem. Phys. Lett. **188**, 21 (1992).
[8] D. J. Evans, Phys. Lett. **91A**, 457 (1982).
[9] J. Casas-Vazquez and D. Jou, Phys. Rev. E **49**, 1040 (1994).
[10] H. Bidar, J. Casas-Vazquez, and D. Jou, Phys. Lett. (to be published).
[11] B. D. Todd, D. J. Evans, and P. J. Daivis (unpublished).